

DYNAMICS OF MICROFLUIDIC MIXING USING TIME PULSING

ARNAUD GOULLET, IAN GLASGOW*, NADINE AUBRY

New Jersey Institute of Technology
University Heights
Newark, NJ 07102, USA

Abstract. Many microfluidic applications require the mixing of reagents, but efficient mixing in these laminar systems remains a challenge. In this paper, we consider further the method of pulsed flow mixing which takes advantage of time dependency rather than spatial complexity. In particular, using computational fluid dynamics (CFD) we analyze the dynamics of the flow when the two inlets are pulsed at 90° and 180° out of phase. Both cases achieve enhanced mixing although better results occur in the first case. This is apparent in the concentration level plots as well as in the shape of material lines which show strong repeated stretching and folding at the confluence region.

1. Introduction. Microfluidics is a growing field, with applications from miniature fuel cells to microarrays for pharmaceutical development and medical diagnostics. Although one of the most basic steps in microfluidic systems is the mixing of reagents, mixing is difficult to achieve at small scale because of the low Reynolds number involved. Several techniques have been developed to address this issue, based upon miniature stirrers [1], external fields [2, 3, 4] or clever geometries [5, 6]. Some of those being quite complicated to implement or difficult to manufacture, one needs to keep in mind that the simplicity of the mixing device, in addition to its efficiency, is a requirement for finding a path to real applications. As in previous works [7, 8] we use here simple geometries with varying flow rates at the inlets. More specifically, we consider the problem of mixing two reagents, denoted A and B, coming separately from two inlets. The two inlet channels merge at 90° to the outlet channel and the mixed solution is “collected” in the outlet channel as in reference [8] (see Figure 1).

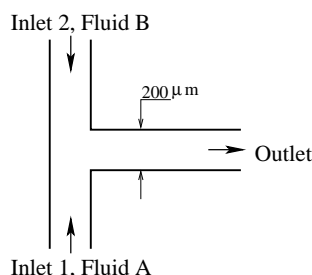


FIGURE 1. Channel geometry.

2000 *Mathematics Subject Classification.* Primary:58F15, 58F17; Secondary: 53C35.

Key words and phrases. microfluidic, mixing.

*Permanent address : Next Advance, Inc., Rensselaer, NY 12144, USA.

Experiments and numerical simulations are performed to study the mixing in the device. The channels are typically $200\ \mu\text{m}$ wide by $120\ \mu\text{m}$ deep. The numerical simulations were run using Fluent 6 (Fluent Inc., Lebanon, NH) and the experimental results were obtained with the experimental set up described in [7, 8]. The results we present here are mostly from the numerical simulations but our experimental results corroborate the CFD simulations. In the case where the flow rate at the inlets is constant, no mixing between the two fluids occurs (see Figure 2), except downstream as the result of diffusion.

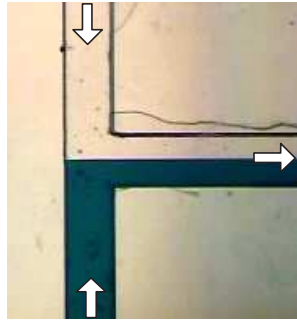


FIGURE 2. Experimental photograph of a steady, unmixed flow obtained when no pulsing is applied. Here, the two fluids used were water in Inlet 2 (top channel) and dyed water in Inlet 1 (bottom channel).

We observe experimentally that introducing a time dependency in the flow rate at the inlets produces mixing in spite of the simplicity of the geometry. Specifically, we superimpose a low frequency sinusoidal flow rate onto a constant mean flow, as illustrated in Figure 3, so that the amplitude of the oscillation is not small and therefore cannot be considered as a perturbation.

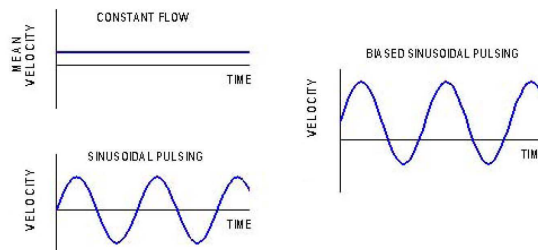


FIGURE 3. Time dependency of the flow rate at one inlet. The biased sinusoidal pulsing consists of a constant flow and a sinusoidal pulsing component.

Since the amplitude is actually chosen larger than the mean flow, the flow in the inlets reverses during a portion of the cycle. This results in some fluid coming back into the inlet channels, while on average the fluid flows downstream toward the outlet. The goal of this paper is to carry out a more complete analysis of the mixing taking place in such a device, particularly from a dynamical systems viewpoint.

2. Numerical simulations. A full three-dimensional (3D) model is used with a hexahedral mesh, with most of the cells having all sides about $10 \mu m$ long. Thus, the channels consist of 20 cells across the channel, 12 cells along the depth, and each cycle is discretized with 40 time steps. The fluids from both inlets are identical but called different names, A and B. The Navier-Stokes equations and diffusion-advection equation are solved in order to determine the concentration distribution inside the device. In our numerical study we take a constant of diffusivity $D = 10^{-10} m^2 s^{-1}$ which is the relevant order of magnitude for many BioMEMS applications.

We can visualize the mixing by plotting the mass fraction of liquid A inside the channel and quantify the efficiency of the mixing by using the degree of mixing [7] defined by,

$$\text{degree of mixing} = 1 - \frac{1}{\mu} \sqrt{\sum_{i=1}^n \frac{(x_i - \mu)^2}{n} \left(\frac{v_i}{v_{mean}} \right)} \quad \text{with } \mu = 0.5. \quad (1)$$

The sum is over the cells of a certain cross section (located in this paper 0.5 mm downstream the confluence of the channels). x_i , v_i represent the mass fraction of liquid A and the velocity at the i^{th} cell, respectively. A non-mixed fluid, therefore, has a degree of mixing equal to zero, and a fully mixed fluid has a degree of mixing equal to 1. While various measures of the degree of mixing can be found in the literature, in this paper we adopt the previous definition based on the standard deviation of a sample of mass fraction of liquid A (in each computational cell) about a fixed value μ and taking into account the various velocities in the different cells [7].

3. Influence of the dimensionless parameters. As in reference [8], we first introduce the different dimensionless parameters of the problem. The Reynolds number or ratio of the importance of the inertial effects with respect to viscous effects, is defined by

$$Re = \frac{VL}{\nu} = 0.3, \quad (2)$$

where V is the mean velocity in the outlet channel, ν is the kinematic viscosity taken to be $10^{-6} m^2 s^{-1}$ for aqueous solutions at room temperature, and L is the hydraulic diameter defined by $(4 \times \text{area}) / (\text{wetted perimeter})$.

The presence of the forcing frequency leads to the Strouhal number, the ratio of the flow characteristic time scale (V/L) to the pulsing time period ($1/f$),

$$St = \frac{fL}{V} = 0.4 \quad \text{for } f=5\text{Hz}. \quad (3)$$

It is also natural to introduce the pulse volume ratio as the volume of fluid displaced per cycle divided by the volume of the confluence region.

$$PVR = \frac{\text{Pulse Volume}}{\text{Intersection Volume}}. \quad (4)$$

In order to test the extent of the mixing and the influence of the former parameters, we consider a phase difference of $\phi = 180^\circ$ between the two inlets. That is, the velocity at the inlets has the form $V_1(t) = 1 + 7.5 \sin(10\pi t)$ (Inlet 1) and $V_2(t) = 1 - 7.5 \sin(10\pi t) \text{ mm.s}^{-1}$ (Inlet 2), respectively, with t representing the time in seconds. Before varying the Strouhal number, we first check if the degree of mixing remains constant when holding the Strouhal number constant while varying the

forcing frequency and the base flow velocity. The data are taken every quarter of a cycle, and Figure 4 shows the variation of the degree of mixing during each cycle. This corroborates the similarity of the flow with the Strouhal number. See also reference ??.

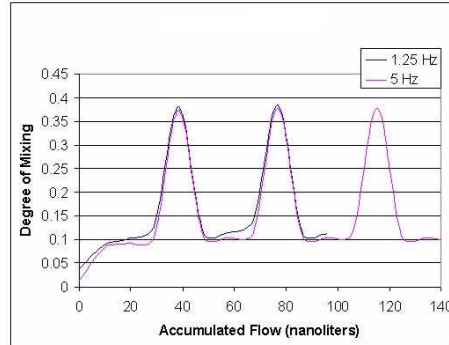


FIGURE 4. Similarity of the degree of mixing for two different frequencies for a Strouhal number equal to 0.094.

We now investigate the influence of the Strouhal number, for a base mean velocity of 1 mm.s^{-1} . The range of Strouhal numbers reported here is from $St = 0.094$ (1.25 Hz) to $St = 1.5$ (20 Hz). Table 1 shows a greater degree of mixing with increasing Strouhal number.

TABLE 1. Degree of mixing versus Strouhal number.

Strouhal number	Degree of mixing
0.094	0.384
0.375	0.703
1.5	0.865

Similarly, the mixing efficiency is seen to improve as the pulse volume ratio increases to a value on the order of one (see Table 2). A more complete discussion regarding the pulse volume ratio can be found in reference [8].

TABLE 2. Degree of mixing versus Pulse Volume Ratio (PVR).

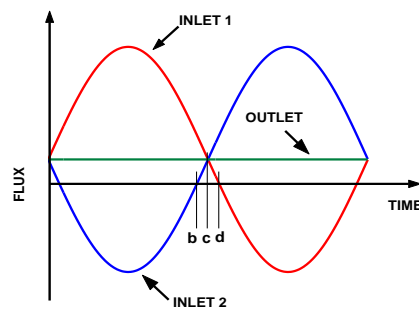
PVR	Degree of mixing
0.47	0.12
1.89	0.72

4. Effect of the phase between the two inlets. Another important parameter of the problem is the phase difference ϕ between the two inlets. For velocities at the inlets defined by $V_1(t) = 1 + 7.5 \sin(10\pi t)$ (Inlet 1) and $V_2(t) = 1 + 7.5 \sin(10\pi t + \phi)$ (Inlet 2), where t is the time in seconds and the velocities are expressed in mm.s^{-1} (thus corresponding to a frequency of 5Hz), we obtain a degree of mixing of 0.66 and 0.63 for $\phi = 90^\circ$ and $\phi = 180^\circ$, respectively. We recall that the recording of the degree of mixing was performed in the cross section located 0.5 mm downstream of the confluence region.

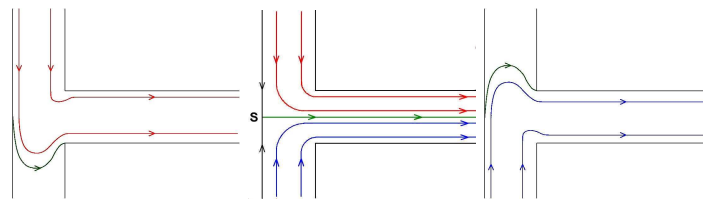
We note that for the case of a phase difference of $\phi = 180^\circ$, the degree of mixing fluctuates in time and the degree of mixing reported corresponds to the time average. In order to understand the difference in this global mixing efficiency between the two cases, we study the flow in more detail taking a dynamical systems approach. In particular, we investigate the time evolution of lines of passive particles, or particle filaments, and record their position after successive pulsing periods. The movement of each particle is determined by integrating the equation of motion $d\mathbf{x}/dt = \mathbf{v}$ where \mathbf{x} is the position vector of the particle and \mathbf{v} is the velocity vector of the fluid at that particular location. From a dynamical systems perspective, we are interested in finding repeated folding and stretching of material lines characteristic of chaotic advection and known to be an effective means of mixing [9, 10]. Due to the complexity of the particles' dynamics in the direction normal to the interface within the confluence area, we carried out numerical simulations with a refined mesh in this particular region to include 120 cells across the channel. The initial condition was a straight line of 2000 particles located in the confluence region.

Case of $\phi = 180^\circ$

With the assumption of incompressibility, the flow rate at the outlet is the sum of the flow rates at the inlets. For this particular case, it follows that the flow rate at the outlet is constant (see Figure 5 (a) which shows the flow rate in the inlets and outlet).



(a)



(b)

(c)

(d)

FIGURE 5. Schematic of the flow in the $\phi = 180^\circ$ case. (a) Flow rate versus time in the two inlets and in the outlet; (b), (c), (d) instantaneous streamlines of the flow at the time points (b), (c), (d) marked in Figure 5a.

We label by “b” “c” and “d” the three time points which are particularly relevant for the dynamics. Instantaneous sets of streamlines at times (b), (c), and (d) are shown in Figure 5(b-d). We start the description of the dynamics when both inlets have the same flow rate (Figure 5 (c)). The lower and upper portions of the flow are images of one another by reflection symmetry, and separated in the mid-plane by a separatrix which ends on the left wall at a stagnation point (saddle point labeled S). The stable manifold of the saddle point is the wall itself and the unstable manifold is the separatrix or interface between the two fluids. Due to the time dependency of the flow rate at the inlets, the separatrix oscillates up and down between two extreme positions shown in Figures 5 (b) and (d). We now consider an initial material line in the confluence area along the unstable manifold (see Figure 6 (a)) and the initial time is taken to match that of Figure 5 (c).

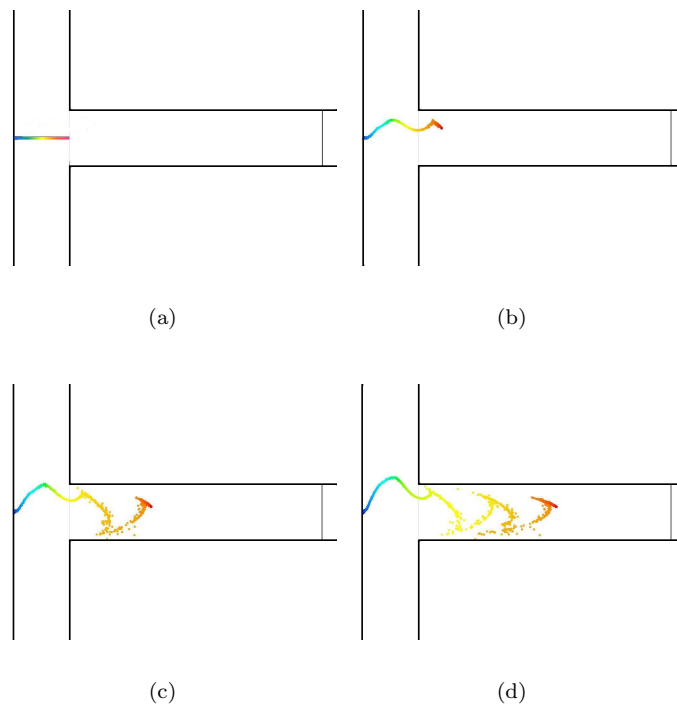


FIGURE 6. Evolution of a material line for $\phi = 180^\circ$. a) Initial condition, b) after 1 period, c) after 2 periods and d) after 3 periods. The vertical line at the outlet is 1 mm downstream from the intersection.

Figures 6 (b)-(d) show a periodic pattern in the material line corresponding to the temporal oscillations of the separatrix, after one, two and three pulse cycles, respectively. Such a pattern corresponds to periodic puffs of liquid A and B in the concentration plot (Figure 7), responsible of the fluctuations of the degree of mixing mentioned before (see also reference [7]). We notice that the amplitude of the pulse is large enough to push the separatrix up so that it eventually touches the upper 90° corner of the wall. By symmetry, the same phenomenon occurs as the separatrix moves down.

The folds form at the intersection and then flow downstream under the action of the mean flow. As the periodic pattern travels downstream, it diffuses slowly. In addition, due to the velocity profile in the outlet channel each puff becomes more and more elongated.

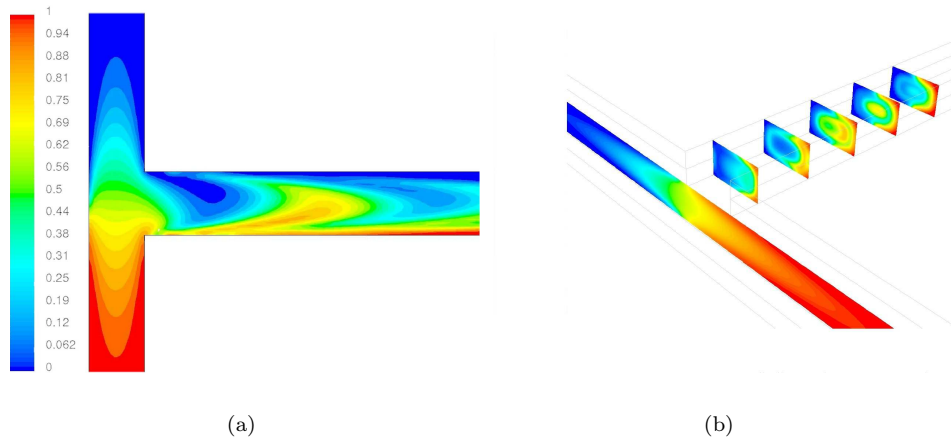


FIGURE 7. Contour plot of concentration of fluid A when the two inlets are pulsed at a $\phi = 180^\circ$ phase difference: a) at half the depth of the channel, b) in various cross-sections of the outlet channel.

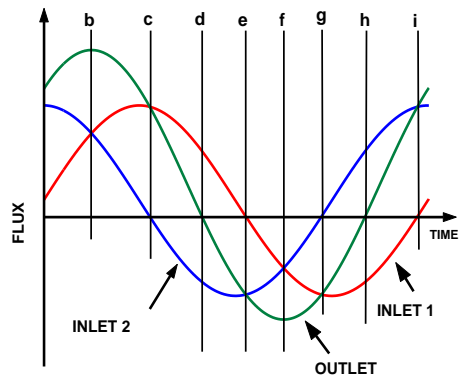
Case of $\phi = 90^\circ$

Another choice consists in imposing a phase difference of $\phi = 90^\circ$, for which we observe that the dynamics at the confluence drastically changes. Notice that in this case the flow rate at the outlet is no longer constant but sinusoidal in time (see Figure 8 (a) showing the flow rate in the two inlets and in the outlet).

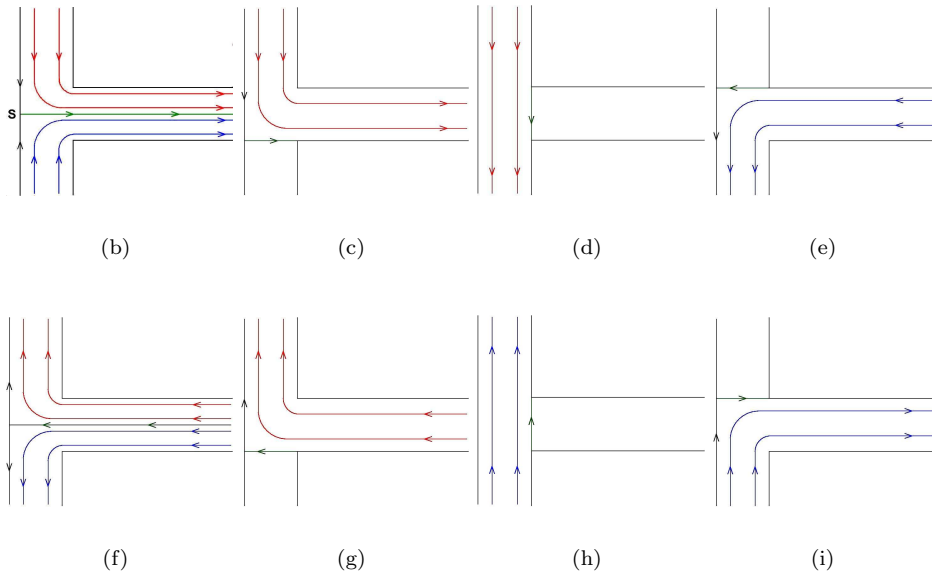
Figure 8 (b)-(i) displays the instantaneous streamlines of the flow for the particular times marked (b)-(i) in Figure 8 (a). In particular, we notice the symmetry of streamline patterns with a reversed direction of the flow in the second part of the cycle.

In this case, the fluid travels back and forth through the confluence region while on average there is still a mean flow downstream. We now consider the initial condition of a line of particles located as indicated in Figure 9 (a). The initial time was chosen with equal flow rates from both inlets corresponding to Figure 8 (b), similar to that of the 180° case.

From Figure 9 (b), we can clearly see the folding of the particle line occurring at the confluence after one period. We notice, however, that the dynamics is not symmetric with respect to the midplane of the channel. In our case, two folds take place, one in the upper inlet and the other one in the outlet channel. In subsequent cycles, the inlet folds always occur in the upper inlet. This is due to the choice in the phase difference and starting point in the cycle. Due to the periodicity in time of the superimposed pulse, the material line stretches and folds in each cycle, bringing the fluid back to the confluence area several times. The base flow, however, keeps the fluid moving downstream, making the front of the folds progress in the downstream direction as time evolves, as they were in Figure 6.



(a)

FIGURE 8. Instantaneous streamlines for $\phi = 90^\circ$.

Such a succession of folds and stretches is typical of chaotic advection, and therefore particles close initially will diverge, thus promoting mixing. The improvement of mixing is also clear from the concentration contour plot shown in Figure 10.

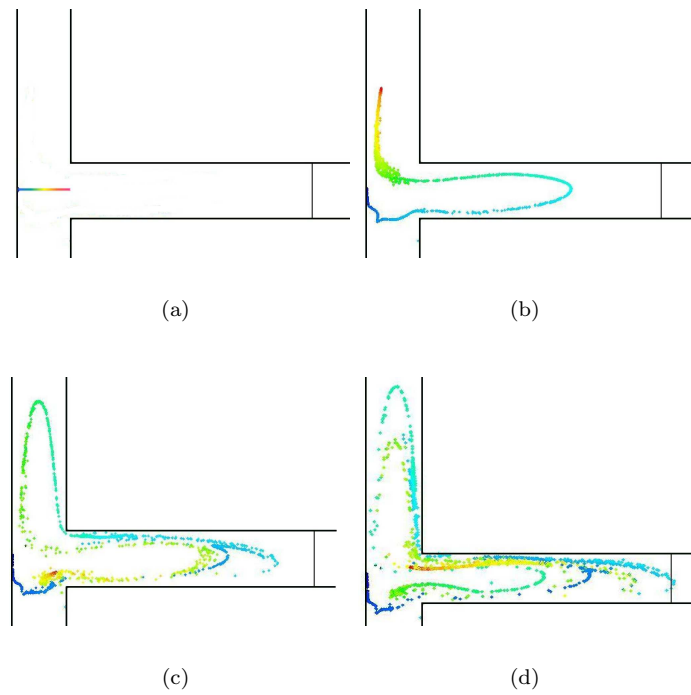


FIGURE 9. Evolution of a material line for $\phi = 90^\circ$. a) Initial condition, b) after 1 period, c) after 2 periods and d) after 3 periods. The vertical line in the outlet channel is placed at the same location as in figure 6.

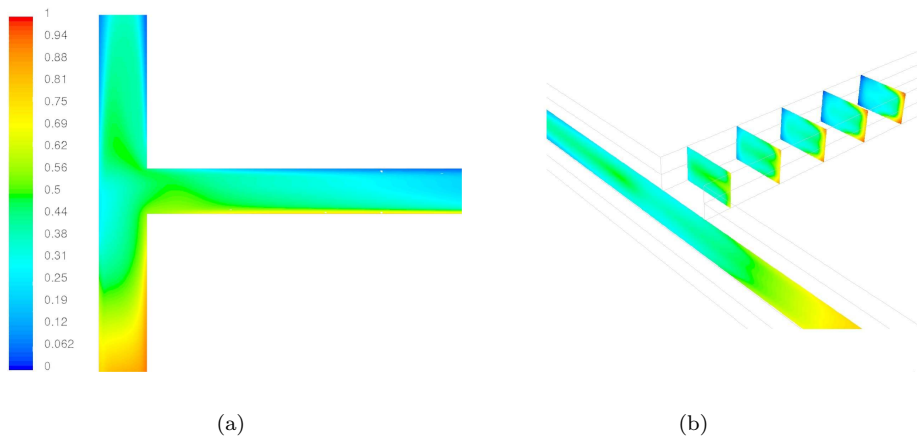


FIGURE 10. Contour plot of concentration of fluid A when the two inlets are pulsed at a $\phi = 90^\circ$ phase difference: a) at half the depth of the channel, b) in various cross-sections of the outlet channel.

5. Conclusion. Adding to a base flow out-of-phase pulsing in inlet channels has a significant influence on the mixing of the two incoming fluids. This was demonstrated for a 180° and 90° phase difference by studying the evolution of concentration contours as well as material lines. The mixing efficiency was shown to be higher and the stretching and folding of material lines stronger in the case of the 90° phase difference.

Acknowledgements. We would like to thank the referees for their valuable comments and suggestions. We are also grateful to the New Jersey Commission for Science and Technology for their financial support through the New Jersey Center for Micro Flow Control (grant # 01-2042-007-25).

REFERENCES

- [1] J.E. Curtis, B.A. Koss and D.G. Grier, *Dynamic holographic optical tweezers*, Opt. Commun, **207** (2002), 169–175.
- [2] R.H. Liu, R. Lenigk, R.L. Druyor-Sanchez, J. Yang and P. Grodzinski, *Hybridization enhancement using cavitation microstreaming*, Anal. Chem., **75** (2003), 1911–1917.
- [3] H.H. Bau, J. Zhong and M. Yi, *A minute magneto hydro dynamic (MHD) mixer*, Sens. Actuators, **79** (2001), 205–213.
- [4] A. Ould El Moctar, N. Aubry and J. Batton, *Electro-hydrodynamic micro-fluidic mixer*, Lab Chip, **3** (2003), 273–280.
- [5] A.D. Stroock, S.K.W. Dertinger, A. Ajdari, I. Mezić, H.A. Stone and G.M. Whitesides, *Chaotic mixer for microchannels*, Science, **295** (2002), 647.
- [6] R.H. Liu, M.A. Stremler, K.V. Sharp, M.G. Olsen, J.G. Santiago, R.J. Adrian, H. Aref and D.J. Beebe, *Passive mixing in a three-dimensional serpentine microchannel*, J. Microelectromechanical Systems, **9** (2000), 190.
- [7] I. Glasgow and N. Aubry, *Enhancement of microfluidic mixing using time pulsing*, Lab Chip, **3** (2003), 114–120.
- [8] I. Glasgow, S. Lieber and N. Aubry, *Parameters influencing pulsed flow mixing in microchannels*, Anal. Chem., **76** (2004), no. 16, 4825–4832.
- [9] H. Aref, *The development of chaotic advection*, Phys. Fluids, **14** (2002), 1315–1325.
- [10] S. Wiggins and J.M. Ottino, *Foundations of chaotic mixing*, Phil. Trans. R. Soc. Lond. A, **362** (2004), 937–970.

Received September, 2004; revised April, 2005.

E-mail address: aubry@adm.njit.edu